Chin. Phys. Lett. **39**, 067101 (2022)

Nontrivial Topological States in $BaSn_5$ Superconductor Probed by de Haas–van Alphen Quantum Oscillations

Lixuesong Han(韩李雪松)[1†], Xianbiao Shi(石贤彪)[2,3†], Jinlong Jiao(焦金龙)[4], Zhenhai Yu(于振海)[1], Xia Wang(王霞)[1,5], Na Yu(余娜)[1,5], Zhiqiang Zou(邹志强)[1,5], Jie Ma(马杰)[4], Weiwei Zhao(赵维巍)[2,3], Wei Xia(夏威)[1,6*], and Yanfeng Guo(郭艳峰)[1,6*]

[1]*School of Physical Science and Technology, ShanghaiTech University, Shanghai 201210, China*
[2]*State Key Laboratory of Advanced Welding & Joining and Flexible Printed Electronics Technology Center, Harbin Institute of Technology, Shenzhen 518055, China*
[3]*Shenzhen Key Laboratory of Flexible Printed Electronics Techniology, Harbin Institute of Technology, Shenzhen 518055, China*
[4]*Key Laboratory of Artificial Structures and Quantum Control (Ministry of Education), School of Physics and Astronomy, Shanghai Jiao Tong University, Shanghai 200240, China*
[5]*Analytical Instrumentation Center, School of Physical Science and Technology, ShanghaiTech University, Shanghai 201210, China*
[6]*ShanghaiTech Laboratory for Topological Physics, ShanghaiTech University, Shanghai 201210, China*

(Received 23 February 2022; accepted 24 April 2022; published online 29 May 2022)

We report the nontrivial topological states in an intrinsic type-Ⅱ superconductor $BaSn_5$ ($T_c \sim 4.4$ K) probed by measuring the magnetization, specific heat, de Haas–van Alphen (dHvA) effect, and by performing first-principles calculations. The first-principles calculations reveal a topological nodal ring structure centered at the H point in the $k_z = \pi$ plane of the Brillouin zone, which could be gapped by spin-orbit coupling (SOC), yielding relatively small gaps below and above the Fermi level of about 0.04 eV and 0.14 eV, respectively. The SOC also results in a pair of Dirac points along the Γ–A direction, located at ∼0.2 eV above the Fermi level. The analysis of the dHvA quantum oscillations supports the calculations by revealing a nontrivial Berry phase originating from the hole and electron pockets related to the bands forming the Dirac cones. Thus, our study provides an excellent avenue for investigating the interplay between superconductivity and nontrivial topological states.

DOI: 10.1088/0256-307X/39/6/067101

The Majorana zero mode, which has been conceived to host potential applications for decoherence topological quantum computation due to its non-Abelian statistics characteristic,[1–6] generally occurs at topological defects such as vortices, boundaries, domain walls, or edges of some effectively spinless superconducting systems with odd-parity triplet pairing symmetry, i.e., topological superconductors (TSCs).[2,5–9] The one-dimensional (1D) p-wave and 2D $p_x \pm ip_y$ superconductors have been proposed for such targets.[9] Unfortunately, the pairing symmetry of a few candidates, such as Sr_2RuO_4, $Cu_xBi_2Se_3$, and $SrxBi_2Se_3$, is still under hot debate.[10] Other ways to create equivalent $p + ip$ pairing superconductivity including the construction of $Bi_2Te_3/NbSe_2$ heterostructure[11–13] and chemically doped superconductors, such as $FeTe_{0.55}Se_{0.45}$,[14–17] $(Li_{0.84}Fe_{0.16})OHFeSe$,[18,19] $CaKFe_4As_4$,[20] and cobalt-doped LiFeAs,[21] have reported to be effective for inducing topological superconductivity. Among them, $FeTe_{0.55}Se_{0.45}$ is most intensively studied. It hosts both topological insulator (TI) and Dirac semimetal (DSM) states, with the latter slightly above the Fermi level (E_F). However, compared with the heterostructures and doped superconductors, intrinsic TSCs are preferable for studying the Majorana zero mode because they are free of the disturbance from complicated interface physics and doping result detects or disorder. Therefore, intrinsic superconductors hosting nontrivial topological states have been the targets because the interplay of nontrivial electronic band topology and superconductivity could constitute an excellent solid environment for the Majorana zero mode.[9] Thus, examining the nontrivial topological states in superconductors is a crucial intergradient for discovering intrinsic TSCs. A series of intrinsic superconductors hosting nontrivial topological states have been investigated before,[22–29] and some of them have been reported as TSCs. [29]

The $BaSn_5$ is an already known tin-rich super-

†Lixuesong Han and Xianbiao Shi contributed equally to this work.
*Corresponding author. Email: xiawei2@shanghaitech.edu.cn; guoyf@shanghaitech.edu.cn
© 2022 Chinese Physical Society and IOP Publishing Ltd

conductor with about 4.4 K superconducting critical temperature T_c.[30] As shown in Fig. 1(a), it demonstrates a peculiar crystal structure, in which the Sn atoms are arranged in graphite-like honeycombs. Two such honeycombs form the hexagonal prisms centered by Ba, which could be viewed as a variant of the well-known MgB_2 family of superconductors. Previous studies suggested the $BaSn_5$ as an s-wave multiband superconductor with an isotropic upper critical field, though its electron–phonon coupling strength is debated.[30–32] More interestingly, van Hove singularity in the density of states arising from the lone pairs was observed, which is usually discussed for high T_c cuprate superconductors rather than such a low T_c intermetallic superconductor.[32] $BaSn_5$ has been less studied despite these interesting properties, particularly considering its electronic band structure. It is a natural inspiration to explore the nontrivial topological states in $BaSn_5$, considering that several compounds with close compositions, such as CaSn, $CaSn_3$, and $BaSn_3$ superconductors,[24–26,33–35] host intriguing nontrivial topological states in the bulk band structures and nontrivial topological surface states. In this study, combining basic characterizations of the superconducting properties, measurements of the dHvA effect, and first-principles calculations, we demonstrated that the s-wave type-Ⅱ $BaSn_5$ superconductor hosts intriguing multiple nontrivial topological states that highly resemble those of $FeTe_{0.55}Se_{0.45}$.[14]

Single $BaSn_5$ crystals were grown using the Sn self-flux method.[31] Figure 1(c) shows an optical picture of a typical crystal. The crystal's crystallographic phase and quality were examined on a Bruker D8 single crystal x-ray diffractometer with Mo K_α ($\lambda = 0.71073$ Å) at 300 K. The result indicates a hexagonal structure with the $P6/mmm$ (No. 191) space group and lattice parameters $a = b = 5.37$ Å, $c = 7.097$ Å, $\alpha = \beta = 90°$, $\gamma = 120°$, which are nicely consistent with the previously reported values.[30] The graphite-like Sn atoms, shown in Figs. 1(a) and 1(b), form a two-dimensional slab of face-sharing hexagonal prisms doubly capped with Ba. The element-resolved energy dispersive spectroscopy (EDS) characterizations on more than ten different areas of several crystal pieces revealed a good stoichiometry of 1 : 5, as shown in Fig. 1(c). The high quality of $BaSn_5$ single crystals could be evidenced by the perfect reciprocal space lattice of the single-crystal x-ray diffraction without any impurities, as shown in Figs. 1(d)–1(f). Magnetization and specific heat measurements were performed on magnetic property and physical property measurement systems from Quantum Design.

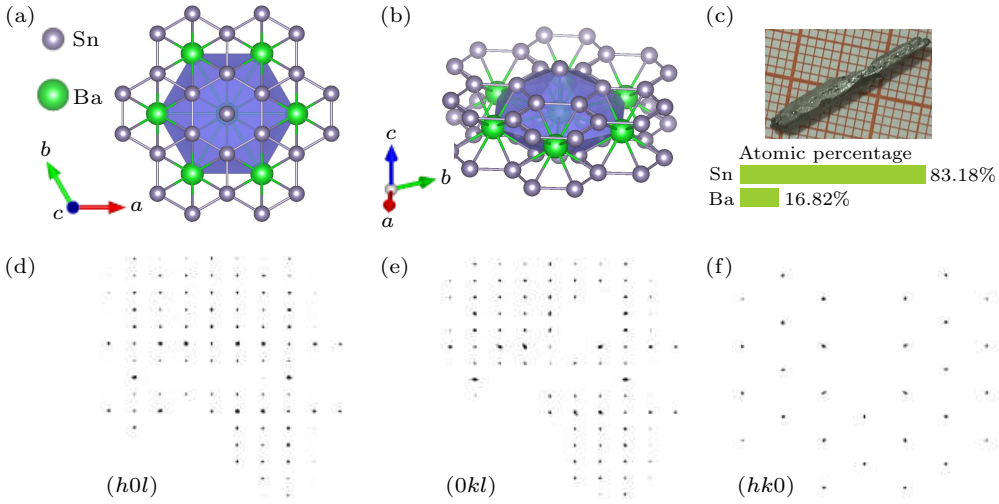

Fig. 1. (a)–(b) Schematic crystal structures of $BaSn_5$ viewed along different orientations. (c) The measured compositions using EDS and an optical picture of a typical $BaSn_5$ crystal. (d)–(f) Diffraction patterns in the reciprocal space along the $(h0l)$, $(0kl)$, and $(hk0)$ directions.

First-principles calculations were performed within the framework of the projector augmented wave method,[36,37] employing the generalized gradient approximation (GGA)[38] with the Perdew–Burke–Ernzerhof formula,[39] as implemented in the Vienna *ab initio* simulation package.[40–42] For all calculations, the cutoff energy for the plane-wave basis was set to 500 eV, the Brillouin zone (BZ) sampling was performed with a Γ-centered Monkhorst–Pack k-point mesh of size $11 \times 11 \times 8$, and the total energy difference criterion was defined as 10^{-8} eV for self-consistent convergence. The optimized structural parameters were used in the electronic structure calculations.

The temperature dependence of the magnetizations with the magnetic field B of 10 Oe applied perpendicular to the (001) plane of the $BaSn_5$ crystal in

the zero-field-cooling (ZFC) and field-cooling modes are illustrated in Fig. 2(a), showing a T_c of ∼4.4 K, consistent with that in the literature.[31] The isothermal magnetizations measured at 2 K are depicted by the inset of Fig. 2(a), indicating a type-Ⅱ superconductivity by the clear hysteresis. Note that, unlike $BaSn_5$, Sn is a type-I superconductor with a $T_c \sim 3.6$ K. Also, the bulk superconductivity is demonstrated by the ∼ 76.3% superconducting shielding volume fraction estimated from the ZFC data at 2 K.

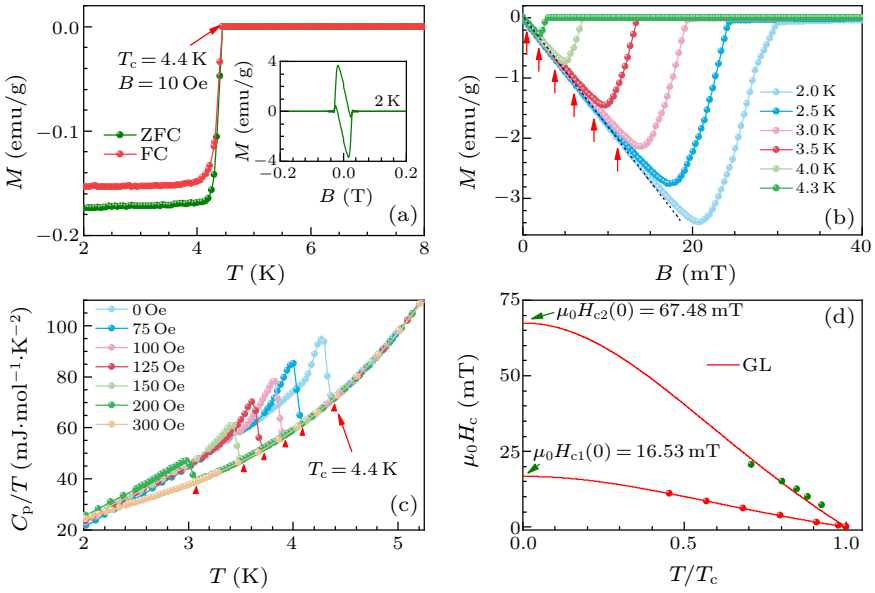

Fig. 2. (a) Temperature dependence of $BaSn_5$ magnetization at 10 Oe. The inset shows the isothermal magnetization at 2 K. (b) Isothermal magnetizations measured at $T = 2$–4.3 K with an interval of 0.5 K. (c) C_p/T around T_c with 0–300 Oe magnetic field. The arrows indicate the positions for the jump. (d) Upper (lower) critical field H_{c2} (H_{c1}) versus the normalized temperature T/T_c. The solid lines denote the fitting results to H_{c2} and H_{c1} using the Ginsburg–Landau (G-L) equation.

The bulk nature of the superconductivity is further confirmed by the evident jump in the specific heat $C_p(T)$ at $B = 0$ T. Moreover, the T_c observed in the $C_p(T)$ is ∼4.4 K, nicely consistent with that derived from the magnetization characterization. To evaluate the lower and upper critical field, the temperature-dependent isothermal magnetizations and magnetic-field-dependent low-temperature specific heat of $BaSn_5$ are presented in Figs. 2(b) and 2(c), respectively. The lower critical magnetic fields H_{c1} were determined using the magnetic field values at which the magnetizations start to deviate from the linear evolution, as shown by the arrows in the inset to Fig. 2(b). This allows the extraction of the $H_{c1}(0)$ via fitting these values by employing the G-L equation $H_{c1}(T) = H_{c1}(0)\frac{1-t^2}{1+t^2}$, where $t = T/T_c$ is the reduced temperature. This yields $H_{c1}(0) = 16.53$ mT. Next, the superconducting jump in $C_p(T)$ exhibits an apparent suppression to low temperatures upon the external magnetic field, allowing the H_{c2}–T diagram to be constructed. By employing the G-L equation $H_{c2}(T) = H_{c2}(0)\frac{1-t^2}{1+t^2}$,[34] the solid line in Fig. 2(d) shows the fitting result. The upper critical magnetic field $H_{c2}(0)$ is 67.48 mT, comparable with previous studies.[31]

The electronic band structure of $BaSn_5$ was studied by performing the first-principles calculations to understand its transport properties. As shown in Fig. 3(a), the $BaSn_5$ band structure, without considering the SOC, manifests a metallic character with several bands crossing the E_F. The enlarged view in Fig. 3(b) shows that two band-crossing points at −0.04 eV along the L–H path and at 0.14 eV along the H–A line are visible in the BZ. The fat band structure shows that the contribution to these crossing bands comes mainly from the Sn 5p states, forming an inverted band structure at the H point. Figure 3(c) shows that the coupling of band-crossing points is not isolated but belong to a nodal ring centered at the H point in the $k_z = \pi$ plane. Therefore, $BaSn_5$ superconductor could be classified into a topological metal with a Dirac nodal ring structure when the SOC is ignored.

When the SOC is considered, as presented in Fig. 3(d), the $BaSn_5$ nodal line is gapped, showing a relatively small gap with a maximum size of about 20 meV along the L–H path of the BZ. This is much smaller than the energy dispersion of the nodal ring (about 180 meV). Moreover, the SOC induces a pair of Dirac points (DPs) along the Γ–A direction, as shown in Fig. 3(f). The DPs located at about 0.2 eV above the E_F can contribute to the transport behavior since

the Dirac cone bands cross the E_F. Hence, the $BaSn_5$ superconductor hosts both the DSM and TI states when the SOC is considered.

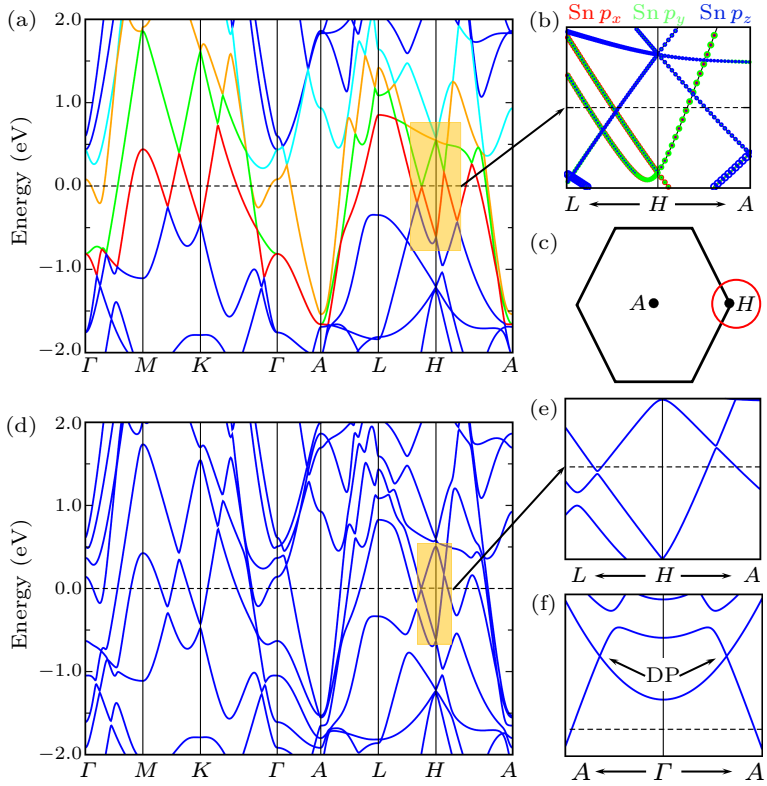

Fig. 3. (a) Electronic band structure of $BaSn_5$ without considering the SOC. (b) Enlarged band structure along the L–H and H–A paths. The symbol size in (b) corresponds to the projected weight of the Bloch states onto the Sn p_x (red), Sn p_y (green), and Sn p_z (blue) orbits. (c) Schematic illustration of the nodal ring centered at the H point in the $k_z = \pi$ plane. (d) Electronic band structure of $BaSn_5$ with the SOC considered. (e) The same as (b) but with the SOC included. (f) Enlarged band structure along the A–Γ path, showing a pair of Dirac points.

Table 1. Parameters derived from dHvA oscillations for $BaSn_5$, where k_F is the Fermi wave vector, v_F denotes the Fermi velocity, τ_Q is the relaxation time, and Φ_B is the Berry phase.

	F (T)	A (nm^{-2})	k_F (nm^{-1})	v_F (m/s)	m^*/m_e	T_D (K)	τ_Q (s)	Φ_B
F_1	21	0.200	0.252	4.3×10^5	0.07	1.792	6.78×10^{-13}	0.508 π
F_2	86.4	0.822	0.512	5.5×10^5	0.11	6.287	1.93×10^{-13}	1.038 π
F_3	103.3	0.985	0.560	5.2×10^5	0.12	9.338	1.30×10^{-13}	1.100 π
F_4	53.3	0.508	0.402	5.8×10^5	0.08	3.84	3.17×10^{-13}	-0.214π
F_5	185	1.764	0.750	1.05×10^6	0.07	21.99	5.5×10^{-14}	1.440 π
F_6	207	1.973	0.793	1.09×10^6	0.07	16.80	7.2×10^{-14}	0.740 π
F_7	561	5.349	1.305	1.59×10^6	0.08	20.11	6.0×10^{-14}	0.452 π

The dHvA effect was measured to probe the Fermi surface (FS) of $BaSn_5$. As shown in Figs. 4(a) and 4(d), we measured the isothermal magnetization of the $BaSn_5$ up to 7 T with $B//[1\bar{1}0]$ and $B//[001]$ at various temperatures. As shown in Figs. 4(b) and 4(e), after subtracting the background, the magnetizations ΔM ($\Delta M = M - M_{\text{background}}$) display striking oscillations in the temperature range 2–30 K, which could be well described by the Lifshitz–Kosevich (L-K) formula[43]

$$\Delta M \propto B^{\lambda} R_T R_D R_S \sin\left[2\pi\left(\frac{F}{B} - \gamma - \delta\right)\right],$$

where $R_T = 2\pi^2 k_B T/[\hbar\omega_c \sinh(2\pi^2 k_B T/\hbar\omega_c)]$ with $\omega_c = eB/m^*$ being the cyclotron frequency and m^* denoting the effective cyclotron mass. $R_D = \exp(-2\pi^2 k_B T_D/\hbar\omega_c)$ with T_D being the Dingle temperature and $R_S = \cos(\pi g m^*/2m_e)$. The index λ is determined by the dimensions, with the λ denoting 1/2 in the three-dimensional (3D) case and 0 in the 2D case.[44] The phase factor $(-\gamma - \delta)$ is used to describe the oscillation part, where $\gamma = 1/2 - \Phi_B/2\pi$, with Φ_B being the Berry phase. The dimension of the FS determines the phase shifts, which takes the value of 0 for the 2D and $\pm 1/8$ ($-$ corresponding to the electron-like pocket and $+$ to the hole-like pocket) for the 3D case. The first-order differential of M vs $1/B$ allows the analysis of the fast Fourier transformation (FFT),

as shown in Figs. 4(c) and 4(f). Multiple fundamental frequencies were obtained when $B//[1\bar{1}0]$ and $B//[001]$, as shown in Figs. 4(c) and 4(f), respectively. For a more accurate fitting, band-pass filtering was performed to separate the low and high-frequency components. Thus, the obtained fundamental frequencies are labeled as F_1 (21 T), F_2 (86.4 T), F_3 (103.3 T), F_4 (53.3 T), F_5 (185 T), F_6 (207 T), and F_7 (561 T). Here, $2F_2$ and $2F_6$ are the harmonic values indicating the same FS for F_2 and F_6. The multiple fundamental frequencies imply that several Fermi pockets are across or close to the E_F. The areas of the Fermi pockets A_F can be calculated using the Onsager relationship $F = A_F(\phi/2\pi^2)$. The effective mass m^* can be obtained by fitting the temperature-dependent oscillation amplitude to the thermal resistance factor R_T, as shown in Figs. 5(b) and 5(e). Figures 5(c) and 5(f) show that the obtained Dingle temperatures T_D are evaluated for the fundamental frequencies F_1–F_7 by fitting the field-dependent amplitude of the quantum oscillations at 2 K. The other parameters are listed in Table 1.

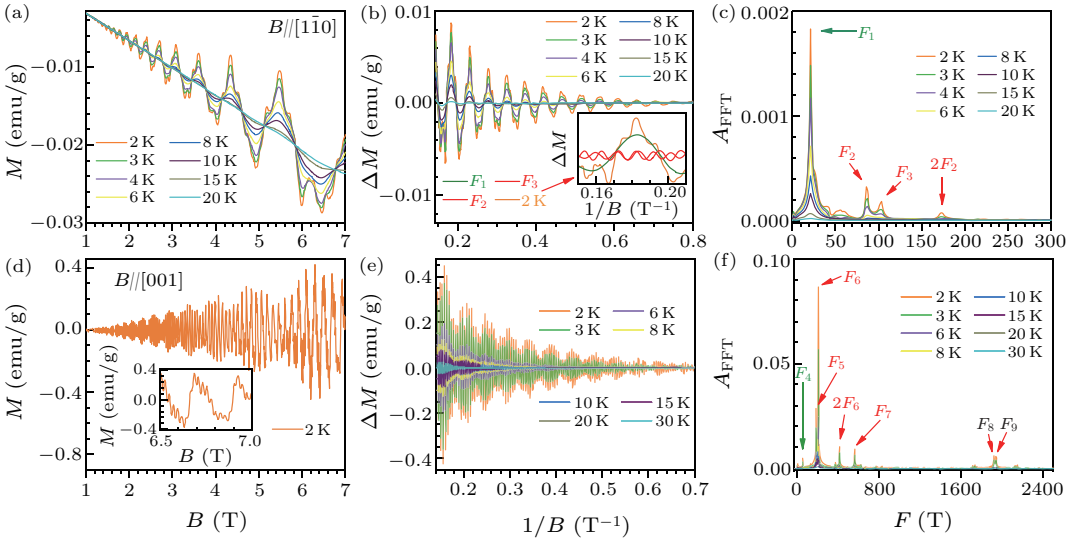

Fig. 4. [(a), (d)] Magnetizations of $BaSn_5$ vs B for $B//[1\bar{1}0]$ and $B//[001]$, respectively, at various temperatures. [(b), (e)] The quantum oscillations for $B//[1\bar{1}0]$ and $B//[001]$ vs $1/B$, respectively, at various temperatures. The inset in (b) shows the three filtered oscillatory parts of ΔM. The orange line represents the raw dHvA oscillatory signal of the $BaSn_5$ at 2 K. [(c), (f)] Fast Fourier transform (FFT) spectra of ΔM at various temperatures.

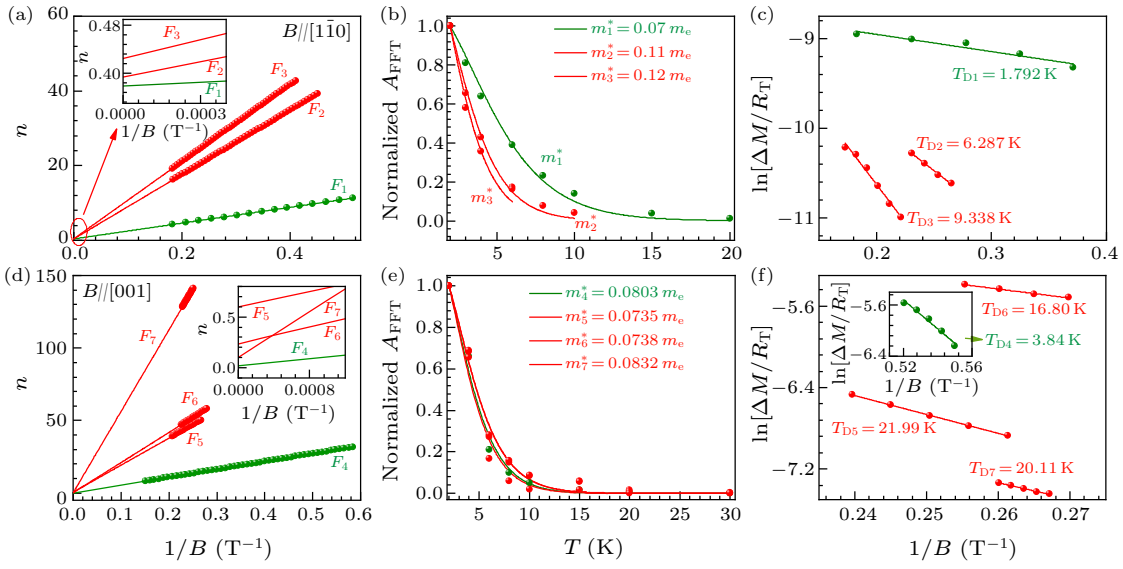

Fig. 5. [(a), (d)] Landau indexes $n = N - \frac{1}{4}$ against $1/B$ at 2 K for $B//[1\bar{1}0]$ and $B//[001]$, respectively. Each inset enlarges the fitting intercept. [(b), (e)] Temperature dependence of relative FFT amplitudes of the oscillations for $B//[1\bar{1}0]$ and $B//[001]$, respectively. [(c), (f)] Dingle plots of dHvA oscillations at 2 K for $B//[1\bar{1}0]$ and $B//[001]$, respectively.

The Landau level (LL) fan diagrams were established to test the Berry phase of the $BaSn_5$ accumulated along with the cyclotron orbit. The LL phase diagrams for F_1–F_3 and F_4–F_7 are shown in Figs. 5(a) and 5(d), respectively, where the valley positions of ΔM correspond to the Landau indices of $n = N - \frac{1}{4}$, and the peak positions of ΔM correspond to the Landau indices of $n = N + \frac{1}{2} - \frac{1}{4}$.[44] The linear fitting intercepts are 0.379, 0.394, 0.425, 0.018, 0.596, 0.245, and 0.101, corresponding to fundamental frequencies from F_1 to F_7, respectively. The data ambiguously unveil the 3D FS of $BaSn_5$. As shown in Fig. 6(b), these angle-dependent frequencies F_1–F_7 are consistent with the calculated values for bands 1, 2, 3, and 4, respectively, as illustrated in Fig. 6(c). The angle-dependent dHvA oscillations could provide further information about the shape of the FS. Figure 6(a) shows the amplitudes of the oscillations versus $1/B$ at various θ and 2 K. For the $BaSn_5$, band 1 (red) contributes hole pockets, whereas bands 2 (blue), 3 (orange), and 4 (olive green) contribute the electron pockets. By carefully comparing the experimental and theoretical values, F_4 and F_1 are assigned to the electron pockets contributed by band 4, while F_5, F_2, F_6, F_3, and F_7 are assigned to the hole pockets contributed by band 1. Thus, the Berry phases of F_1–F_7 are $2\times(0.379-0.125)\pi$, $2\times(0.394+0.125)\pi$, $2\times(0.425+0.125)\pi$, $2\times(0.018-0.125)\pi$, $2\times(0.596+0.125)\pi$, $2\times(0.245+0.125)\pi$, and $2\times(0.101+0.125)\pi$, respectively. The F_2 and F_3 Berry phases are close to π, indicating the nontrivial topological nature of band 1, consistent with the first-principle calculations. The Berry phases for F_5, F_6, and F_7, which are 1.44π, 0.74π, and 0.456π, respectively, deviate clearly from π, which may be due to their N to be too large, consequently increasing the uncertainty of the fits. However, since F_5, F_2, F_6, F_3, and F_7 are assigned to the hole pockets contributed by band 1, which forms the Dirac nodal ring, the Berry phases for the three fundamental frequencies derived from the quantum oscillations measured at a higher magnetic field should be close to π.

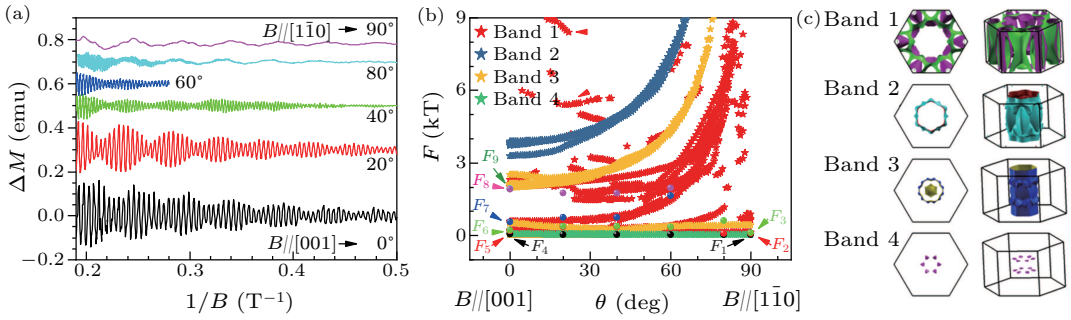

Fig. 6. (a) FFT spectra of ΔM at different θ from $B//[001]$ to $B//[1\bar{1}0]$. (b) Comparison between experimental and theoretical values of the fundamental frequencies with various θ. (c) The calculated FS, in which band 1 contributes to the hole pocket, whereas bands 2, 3, and 4 contribute to the electron pockets.

In summary, we have demonstrated the nontrivial topological states in the $BaSn_5$ superconductor. The characterization by magnetization and specific heat measurements unveils the type-Ⅱ superconductor nature. The dHvA quantum oscillations and first-principles calculations suggest a topological nodal-line structure in $BaSn_5$, which can be gapped by considering the SOC. Alternatively, a pair of DPs appears. Thus, it is interesting that $BaSn_5$ hosts both the TI and DSM states in the electronic band structure, highly resembling the case in $FeTe_{0.55}Se_{0.45}$ and the cobalt-doped LiFeAs.[14,21] If the FS formed by the Dirac Fermi arc can corporate with the bulk superconductivity, it could form an effective proximity effect in momentum space, serving as the solid environment for the Majorana zero mode. Comparing the $BaSn_3$ and $CaSn_3$,[24,35] we can realize that the DPs are closer to the E_F in the $BaSn_5$. This provides an excellent example for studying the correlation between the nontrivial topological states and conventional superconductivity.

Acknowledgments. This work was supported by the National Natural Science Foundation of China (Grant Nos. 92065201, 11774223, and U2032213), the Open Project of Key Laboratory of Artificial Structures and Quantum Control (Ministry of Education), Shanghai Jiao Tong University (Grant No. 2020–04). W.W.Z. was supported by the Shenzhen Peacock Team Plan (Grant No. KQTD20170809110344233) and Bureau of Industry and Information Technology of Shenzhen through the Graphene Manufacturing Innovation Center (Grant No. 201901161514). The authors thank the support from Analytical Instrumentation Center, SPST, ShanghaiTech University (Grant No. SPST-AIC10112914).

References

[1] Wilczek F 2009 *Nat. Phys.* **5** 614
[2] Sato M and Ando Y 2017 *Rep. Prog. Phys.* **80** 076501

[3] Stern A 2010 *Nature* **464** 187
[4] Nayak C, Simon S H, Stern A, Freedman M and Das S S 2008 *Rev. Mod. Phys.* **80** 1083
[5] Qi X L and Zhang S C 2011 *Rev. Mod. Phys.* **83** 1057
[6] Leijnse M and Flensberg K 2012 *Semicond. Sci. Technol.* **27** 124003
[7] Kopnin N B and Salomaa M M 1991 *Phys. Rev. B* **44** 9667
[8] Read N and Green D 2000 *Phys. Rev. B* **61** 10267
[9] Fu L and Kane C L 2008 *Phys. Rev. Lett.* **100** 096407
[10] Mackenzie A P and Maeno Y 2003 *Rev. Mod. Phys.* **75** 657
[11] Wang M X, Liu C, Xu J P, Yang F, Miao L, Yao M Y, Gao C L, Shen C, Ma X, Chen X, Xu Z A, Liu Y, Zhang S C, Qian D, Jia J F and Xue Q K 2012 *Science* **336** 52
[12] Xu J P, Wang M X, Liu Z L, Ge J F, Yang X, Liu C, Xu Z A, Guan D, Gao C L, Qian D, Liu Y, Wang Q H, Zhang F C, Xue Q K and Jia J F 2015 *Phys. Rev. Lett.* **114** 017001
[13] Sun H H, Zhang K W, Hu L H, Li C, Wang G Y, Ma H Y, Xu Z A, Gao C L, Guan D D, Li Y Y, Liu C, Qian D, Zhou Y, Fu L, Li S C, Zhang F C and Jia J F 2016 *Phys. Rev. Lett.* **116** 257003
[14] Zhang P, Yaji K, Hashimoto T, Ota Y, Kondo T, Okazaki K, Wang Z, Wen J, Gu G D, Ding H and Shin S 2018 *Science* **360** 182
[15] Wang Z, Zhang P, Xu G, Zeng L K, Miao H, Xu X, Qian T, Weng H, Richard P, Fedorov A V, Ding H, Dai X and Fang Z 2015 *Phys. Rev. B* **92** 115119
[16] Kong L, Zhu S, Papaj M, Chen H, Cao L, Isobe H, Xing Y, Liu W, Wang D, Fan P, Sun Y, Du S, Schneeloch J, Zhong R, Gu G, Fu L, Gao H J and Ding H 2019 *Nat. Phys.* **15** 1181
[17] Wang D, Kong L, Fan P, Chen H, Zhu S, Liu W, Cao L, Sun Y, Du S, Schneeloch J, Zhong R, Gu G, Fu L, Ding H and Gao H J 2018 *Science* **362** 333
[18] Chen C, Liu Q, Zhang T Z, Li D, Shen P P, Dong X L, Zhao Z X, Zhang T and Feng D L 2019 *Chin. Phys. Lett.* **36** 057403
[19] Liu Q, Chen C, Zhang T, Peng R, Yan Y J, Wen C H P, Lou X, Huang Y L, Tian J P, Dong X L, Wang G W, Bao W C, Wang Q H, Yin Z P, Zhao Z X and Feng D L 2018 *Phys. Rev. X* **8** 041056
[20] Liu W, Cao L, Zhu S, Kong L, Wang G, Papaj M, Zhang P, Liu Y B, Chen H, Li G, Yang F, Kondo T, Du S, Cao G H, Shin S, Fu L, Yin Z, Gao H J and Ding H 2020 *Nat. Commun.* **11** 5688
[21] Kong L, Cao L, Zhu S, Papaj M, Dai G, Li G, Fan P, Liu W, Yang F, Wang X, Du S, Jin C, Fu L, Gao H J and Ding H 2021 *Nat. Commun.* **12** 4146
[22] Xia W, Shi X B, Zhang Y, Su H, Wang Q, Ding L C, Chen L M, Wang X, Zou Z Q, Yu N, Pi L, Hao Y F, Li B, Zhu Z W, Zhao W W, Kou X F and Guo Y F 2020 *Phys. Rev. B* **101** 155117
[23] Chen C, Liang A J, Liu S, Nie S M, Huang J W, Wang M X, Li Y W, Pei D, Yang H F, Zheng H J, Zhang Y, Lu D H, Hashimoto M, Barinov A, Jozwiak C, Bostwick A, Rotenberg E, Kou X F, Yang L X, Guo Y F, Wang Z J, Yuan H T, Liu Z K and Chen Y L 2020 *Matter* **3** 2055
[24] Zhang G N, Shi X B, Liu X L, Xia W, Su H, Chen L M, Wang X, Yu N, Zou Z Q, Zhao W W and Guo Y F 2020 *Chin. Phys. Lett.* **37** 087101
[25] Huang Z, Shi X B, Zhang G N, Liu Z T, Soohyun C, Jiang Z C, Liu Z H, Liu J S, Yang Y C, Xia W, Zhao W W, Guo Y F and Shen D W 2021 *Chin. Phys. Lett.* **38** 107403
[26] Huang K, Luo A Y, Chen C, Zhang G N, Liu X L, Li Y W, Wu F, Cui S T, Sun Z, Jozwiak C, Bostwick A, Rotenberg E, Yang H F, Yang L X, Xu G, Guo Y F, Liu Z K and Chen Y L 2021 *Phys. Rev. B* **103** 155148
[27] Xu L X, Xia Y Y Y, Liu S, Li Y W, Wei L Y, Wang H Y, Wang C W, Yang H F, Liang A J, Huang K, Deng T, Xia W, Zhang X, Zheng H J, Chen Y J, Yang L X, Wang M X, Guo Y F, Li G, Liu Z K and Chen Y L 2021 *Phys. Rev. B* **103** L201109
[28] Yang H F, Liu X L, Nie S M, Shi W J, Huang K, Zheng H J, Zhang J, Li Y W, Liang A J, Wang M X, Yang L X, Guo Y F, L, Z K and Chen Y L 2021 *Phys. Rev. B* **104** L220501
[29] Yuan Y, Pan J, Wang X, Fang Y, Song C, Wang L, He K, Ma X, Zhang H, Huang F, Li W and Xue Q K 2019 *Nat. Phys.* **15** 1046
[30] Fässler T F, Hoffmann S and Kronseder C 2001 *Z. Anorg. Allg. Chem.* **627** 2486
[31] Lin X, Bud'ko S L and Canfield P C 2012 *Philos. Mag.* **92** 3006
[32] Billington D, Ernsting D, Millichamp T E and Dugdale S B 2015 *Philos. Mag.* **95** 1728
[33] Siddiquee K A M H, Munir R, Dissanayake C, Hu X Z, Yadav S, Takano Y, Choi E S, Le D, Rahman T S and Nakajima Y 2021 arXiv:2103.08039v1
[34] Siddiquee K A M H, Munir R, Dissanayake C *et al.* 2019 arXiv:1901.02087v1
[35] Luo X, Shao D F, Pei Q L, Song J Y, Hu L, Han Y Y, Zhu X B, Song W H, Lu W J and Sun Y P 2015 *J. Mater. Chem. C* **3** 11432
[36] Blöchl P E 1994 *Phys. Rev. B* **50** 17953
[37] Lehtomäki J, Makkonen I, Caro M A, Harju A and Lopez-Acevedo O J 2014 *Chem. Phys.* **141** 234102
[38] Perdew J P, Burke K and Ernzerhof M 1996 *Phys. Rev. Lett.* **77** 3865
[39] Perdew J P and Wang Y 1992 *Phys. Rev. B* **45** 13244
[40] Kresse G and Hafner J 1993 *Phys. Rev. B* **47** 558
[41] Kresse G and Furthmüller J 1996 *Comput. Mater. Sci.* **6** 15
[42] Kresse G and Furthmüller J 1996 *Phys. Rev. B* **54** 11169
[43] Mikitik G P and Sharlai Y V 1999 *Phys. Rev. Lett.* **82** 2147
[44] Hu J, Tang Z, Liu J, Liu X, Zhu Y, Graf D, Myhro K, Tran S, Lau C N, Wei J and Mao Z 2016 *Phys. Rev. Lett.* **117** 016602